

# Spin Mode-Switching at the Edge of a Quantum Hall System

Udit Khanna,<sup>1,2</sup> Ganpathy Murthy,<sup>3</sup> Sumathi Rao,<sup>1,2</sup> and Yuval Gefen<sup>4</sup>

<sup>1</sup>Harish-Chandra Research Institute, Chhatnag Road, Jhansi, Allahabad 211019, India

<sup>2</sup>Homi Bhabha National Institute, Training School Complex, Anushaktinagar, Mumbai, Maharashtra 400085, India

<sup>3</sup>Department of Physics and Astronomy, University of Kentucky, Lexington KY 40506-0055, USA

<sup>4</sup>Department of Condensed Matter Physics, Weizmann Institute, 76100 Rehovot, Israel

(Dated: August 29, 2018)

Quantum Hall states can be characterized by their chiral edge modes. Upon softening the edge potential, the edge has long been known to undergo spontaneous reconstruction driven by charging effects. In this paper we demonstrate a qualitatively distinct phenomenon driven by exchange effects, in which the *ordering* of the edge modes at  $\nu = 3$  switches abruptly as the edge potential is made softer, while the ordering in the bulk remains intact. We demonstrate that this phenomenon is robust, and has many verifiable experimental signatures in transport.

PACS numbers: 73.21.-b, 73.22.Gk, 73.43.Lp, 72.80.Vp

Shortly after the discovery of the integer quantum Hall effect (QHE) it was realized that the edges of an incompressible electron gas play a crucial role in transport [1]. In a quantum Hall state, the bulk has a charge gap. Near a sharp edge, gapless chiral modes (described as chiral Luttinger liquids [2]) carry the current between the contacts, consistent with the topologically protected transport observables of the QHE.

In the early 90s it was realized that both integer [3–5] and fractional [6, 7] edges reconstruct as the slope of the edge confining potential  $V_{\text{edge}}(y)$  is made smoother. Reconstruction is the modification of the position and/or the number and nature of the edge modes [3–9]. Subsequently, various manifestations of edge reconstruction have been observed in the QHE regime [10–14], and theoretically studied in many QHE states [15–20] and in time reversal invariant topological insulators [21].

Edge reconstruction is driven by charge effects [22], as seen by the work of Dempsey *et al.* [4] who studied the unpolarized filling factor  $\nu = 2$ . For a sharp edge, the  $n = (0\uparrow)$  and the  $n = (0\downarrow)$  single-particle levels cross the chemical potential  $\mu$  at the same location, with a sharp change in electron density there. As  $V_{\text{edge}}(y)$  is made smoother, the  $\uparrow$  and  $\downarrow$  crossing points spontaneously move away from each other. The occupations now go from  $\nu = 2 \rightarrow \nu = 1 \rightarrow \nu = 0$  as one moves towards the edge, resulting in a smoother change in electron density, which is better able to neutralize the positive background.

In this work we focus on the edge of a  $\nu = 3$  quantum Hall state and uncover edge phenomena driven by spin exchange rather than charge effects [22]. The bulk remains inert at the parameters we consider and only the edge shows a phase transition. We find that, depending on parameters, the order of the two inner or the two outer edge channels switches as  $V_{\text{edge}}(y)$  becomes smoother. The charge density does not change significantly through the transition; no charge reconstruction is observed in the regime where *spin-mode-switching* occurs.

Our (approximate) theoretical analyses indicate that the phase transitions are first-order. In designed geometries with controlled edge steepness and quantum point contacts (QPCs), a host of phenomena can serve as “smoking gun” tests of spin-mode-switching. These include a change in the nature of the spin transport through a single QPC system with and without spin-mode-switching, and a qualitative change in the way disorder affects transport following a spin-mode-switching transition.

To set the stage for our model, we define the cyclotron energy  $\hbar\omega_c = \frac{\hbar eB}{m_b}$  ( $m_b$  is the band mass), the interaction scale  $E_c = \hbar\omega_c \tilde{E}_c = \frac{e^2}{4\pi\epsilon\ell}$  where  $\epsilon$  includes the dielectric constant of the medium, and  $\ell = \sqrt{\hbar/eB}$ , the magnetic length. We will work at tiny Zeeman coupling  $E_z \ll E_c$ .

In the Landau gauge  $eA_x = -\frac{y}{\ell^2}$ ,  $eA_y = 0$ , the single-particle wavefunctions of the  $n^{\text{th}}$  Landau level (LL) in a system with periodic boundary conditions in  $x$  can be written as [23]

$$\Phi_{nk}(x, y) = \frac{e^{ikx} e^{-\frac{(y-k\ell^2)^2}{2\ell^2}}}{\sqrt{2^n n! L_x \ell \sqrt{\pi}}} H_n\left(\frac{y-k\ell^2}{\ell}\right), \quad (1)$$

where  $k = 2\pi m/L_x$  determines the position of the guiding center along the  $y$ -axis. The Hamiltonian of the system  $H = H_b + H_{e\text{-bg}}$  can be split into an electronic bulk part  $H_b$  and the electron-background interaction  $H_{e\text{-bg}}$  responsible for the confining potential  $V_{\text{edge}}$  at the edge. The bulk Hamiltonian is

$$H_b = \hbar\omega_c \sum_{nks} n c_{nks}^\dagger c_{nks} + \frac{1}{2L_x L_y} \sum_{\vec{q}} v(q) : \rho_e(\vec{q}) \rho_e(-\vec{q}) : \quad (2)$$

where the electron density operator  $\rho_e(x, y) = \sum_s \Psi_s^\dagger(x, y) \Psi_s(x, y)$ ,  $\Psi_s(x, y) = \sum_{n,k} \Phi_{nk}(x, y) c_{nks}$ , with  $c_{nks}$  being canonical fermion operators, and  $v(q)$  and  $\rho_e(\vec{q})$  are the Fourier transforms of the interaction  $v(\vec{r} - \vec{r}')$  and  $\rho_e(x, y)$ . The possible translation-invariant ground states of the  $\nu = 3$  bulk are  $|\psi_1\rangle = |0\uparrow, 0\downarrow, 1\uparrow\rangle$

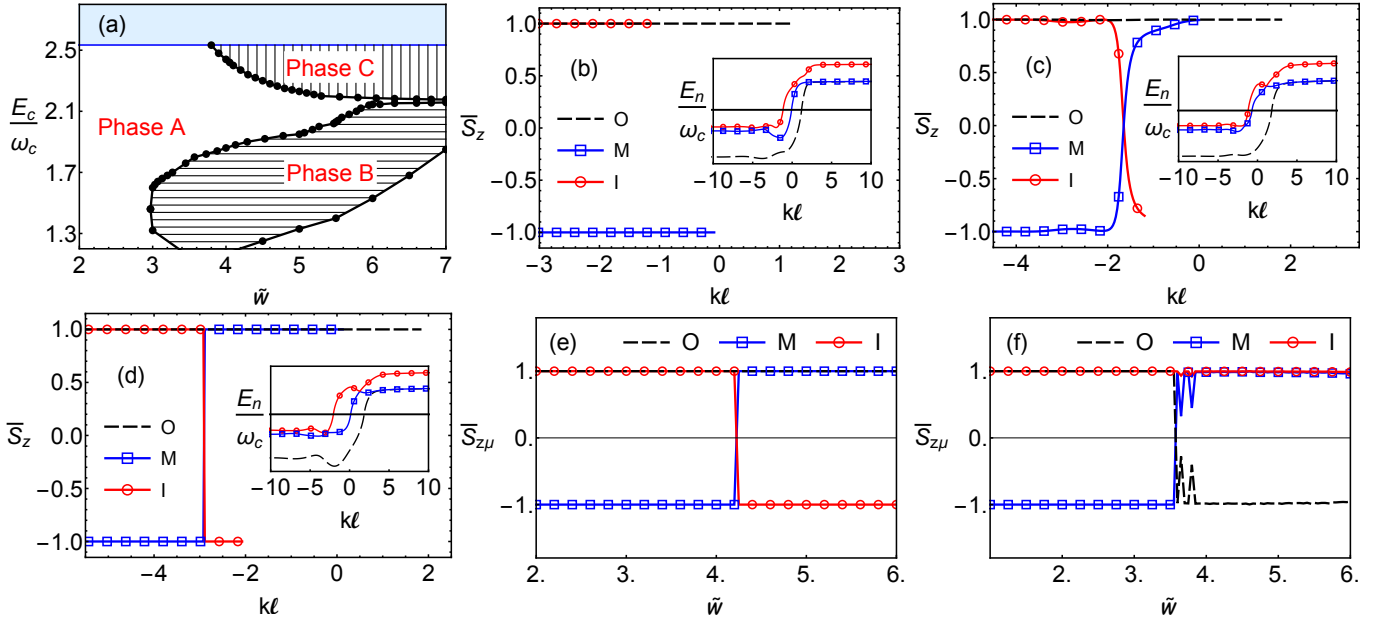


FIG. 1. (Color online) (a) The phase diagram. The background color represents the bulk phase, white being partially polarized ( $|0\uparrow, 0\downarrow, 1\uparrow\rangle$ ) and blue being fully polarized ( $|0\uparrow, 1\uparrow, 2\uparrow\rangle$ ). States are labelled  $i = O$  (outermost),  $M$  (middle) and  $I$  (innermost). The plain white region also denotes edge Phase A ( $O=0\uparrow$ ,  $M=0\downarrow$  and  $I=1\uparrow$ ). Edge Phase B ( $O=0\downarrow$ ,  $M=0\uparrow$  and  $I=1\uparrow$ ) is horizontally hatched, while Phase C ( $O=0\uparrow$ ,  $M=1\uparrow$  and  $I=0\downarrow$ ) is vertically hatched. Due to poor convergence of the HF, for  $6 \leq \tilde{w} \leq 7$ ,  $\tilde{E}_c \simeq 2.13$  it is not clear whether there is a direct transition between Phases B and C, or whether Phase A intervenes. In Figs. 1(b), 1(c) and 1(d) we depict  $\bar{S}_z(i, k)$  of the occupied single-particle states versus  $k\ell$  at  $\tilde{E}_c = 2.3$ . Only occupied levels are depicted. The line for level  $i$  terminates where the level  $i$  crosses  $\mu$ , with  $\bar{S}_z(i, k)$  at the  $\mu$ -crossing defined as  $\bar{S}_{z\mu}(i)$ . The insets depict the energy dispersions of the HF single-particle states vs.  $k\ell$ , with the horizontal black line being  $\mu$ . In Fig. 1(b) we are in Phase A ( $\tilde{w} = 2.0$ ) where no spin rotations occur. Fig. 1(c) shows  $\bar{S}_z(i, k)$  vs.  $k\ell$  at the transition ( $\tilde{w} = 4.28$ ), with spin rotations occurring over a scale  $\ell$ , where the corresponding energy level dispersions come close together in an avoided crossing (inset). Fig. 1(d) shows  $\bar{S}_z(i, k)$  vs.  $k\ell$  in Phase C ( $\tilde{w} = 5.0$ ). The spin rotations are quite abrupt, and occur where the corresponding dispersions undergo a sharp avoided crossing. In Fig. 1(e) we plot  $\bar{S}_{z\mu}(i)$  vs.  $\tilde{w}$  at  $\tilde{E}_c = 2.3$ . A discontinuous change in  $\bar{S}_{z\mu}$  for the  $M$  and  $I$  levels is seen at the transition between Phases A and C. Similar results hold at  $\tilde{E}_c = 1.8$  for the Phase A to Phase B transition, with  $\bar{S}_{z\mu}$  showing a discontinuous change for the  $O$  and  $M$  levels, as shown in Fig. 1(f).

(partially polarized) and  $|\psi_2\rangle = |0\uparrow, 1\uparrow, 2\uparrow\rangle$  (fully polarized), where we write only the spin-labelled LLs that are occupied. As  $\tilde{E}_c$  increases there is a bulk first-order transition [24–26] driven by exchange from  $|\psi_1\rangle$  to  $|\psi_2\rangle$ . In the Hartree-Fock (HF) approximation this occurs at  $\tilde{E}_c \approx 2.5$  for the Coulomb interaction.

The electron-background interaction is

$$H_{e-\text{bg}} = - \int d^2r d^2r' \rho_b(y') v(\vec{r} - \vec{r}') \rho_e(x, y) \quad (3)$$

where  $\rho_b(y)$  is the positive background density which gives rise to the edge confining potential  $V_{\text{edge}}(y) = - \int d^2r' \rho_b(y') v(\vec{r} - \vec{r}')$ . In our model the background density decreases linearly to zero over a distance  $W$  at the edge [5]. The dimensionless parameter  $\tilde{w} = W/\ell$  characterizes the slope of  $V_{\text{edge}}$ ,

$$\rho_b(y) = \begin{cases} \rho_0 & y < -\frac{W}{2} \\ \rho_0 \frac{\frac{W}{2} - y}{W} & -\frac{W}{2} < y < \frac{W}{2} \\ 0 & y > \frac{W}{2} \end{cases}. \quad (4)$$

The rest of the paper is devoted to our theoretical

evidence for spin mode-switching and its robustness to mixing with higher LLs, Zeeman coupling, and varying the interaction parameters. We also propose a set of charge and spin transport experiments to detect spin-mode-switched phases.

*Theoretical Analysis:* Our primary tool is the spin-unrestricted Hartree-Fock (HF) approximation keeping up to 6 spin resolved LLs to include the effect of LL-mixing and spin-mixing. In the HF approximation, the many-body state is replaced by a variational Slater determinant, characterized by all possible averages  $\langle c_i^\dagger c_j \rangle$ . We confine ourselves to translation invariant states:

$$\langle c_{nks}^\dagger c_{n'k's'} \rangle = \delta_{kk'} \Delta_{ns, n's'}(k). \quad (5)$$

In the bulk the matrix  $\Delta_{ns, n's'}$  is independent of  $k$  and diagonal in  $n$  as well as in  $s$  (no LL-mixing or spin-mixing). Near the edge  $\Delta_{ns, n's'}$  acquires a  $k$ -dependence, and LL-mixing/spin-mixing will occur. The optimal Slater determinant that minimizes the variational energy is found by an iterative procedure carried out to self-consistency. At each step, a one-body Hamiltonian (where the interac-

tion term has been replaced by effective one-body terms dependent on  $\Delta_{n_s, n'_s}(k)$  is solved and the energy levels filled up to a chemical potential chosen to satisfy overall charge neutrality. The new state enables the computation of a new set of  $\Delta$ , giving the seed for the next iterative step [27]. The results of the HF calculation are shown in Fig. 1. We use a screened Coulomb interaction of the form  $v(\vec{q}) = \frac{2\pi E_c}{q+q_{sc}}$ , where  $q_{sc}$  is the inverse screening length. The results shown are for  $q_{sc}\ell = 10^{-2}$ , though spin-mode-switching persists at least up to  $q_{sc}\ell = 0.5$ . In unrestricted HF single-particle levels generically cannot be labelled by spin and cannot cross due to level repulsion. We therefore label the edge modes by their location as  $i = \text{O}$  (outermost),  $\text{M}$  (middle) and  $\text{I}$  (innermost). To proceed further, we compute the quantum expectation value  $\bar{S}_z(i, k)$  for each occupied single-particle state  $i$  at position  $k\ell$ . The spin character of the chiral edge modes transporting current are determined by the  $\bar{S}_z(i, k)$  of the corresponding single-particle levels at the crossing with the chemical potential,  $\bar{S}_{z\mu}(i)$ . This allows us to label an edge mode with a spin.

Fig. 1(a) shows two edge-mode-switched phases. For  $\tilde{w} \lesssim 3$ , there is no spin-mixing, and the edges follow the bulk order:  $\text{O}=0\uparrow$ ,  $\text{M}=0\downarrow$  and  $\text{I}=1\uparrow$ . This is Phase A. For  $1.5 \lesssim \tilde{E}_c \lesssim 2.13$  and  $\tilde{w} > 3$ , the system enters Phase B where the order of the edge modes is  $\text{O}=0\downarrow$ ,  $\text{M}=0\uparrow$  and  $\text{I}=1\uparrow$ . Edge Phase C occurs for  $2.13 < \tilde{E}_c < 2.5$  and  $\tilde{w} > 3.5$ , with the edge mode ordering  $\text{O}=0\uparrow$ ,  $\text{M}=1\uparrow$  and  $\text{I}=0\downarrow$ . For  $6 \leq \tilde{w} \leq 7$ ,  $\tilde{E}_c \simeq 2.13$  HF converges poorly, making it unclear whether there is a direct transition between Phases B and C, or whether a sliver of Phase A persists between them. Fig. 1(b) shows  $\bar{S}_z$  vs.  $k\ell$  of the three occupied levels near the edge at  $\tilde{E}_c = 2.3$ ,  $\tilde{w} = 2.0$  (Phase A). The lines terminate where the corresponding level crosses  $\mu$ . Fig. 1(b) inset shows the energy dispersions of the self-consistent HF states for the same parameters. Fig. 1(c) shows  $\bar{S}_z$  vs.  $k\ell$  at the  $A \rightarrow C$  transition ( $\tilde{w} = 4.28$ ), and Fig. 1(d) shows the same in

Phase C ( $\tilde{w} = 5.0$ ). Figs. 1(e), 1(f) show the expectation value  $\bar{S}_{z\mu}$  of the respective levels of O, M and I that intersect the Fermi energy as a function of  $\tilde{w}$  at  $\tilde{E}_c = 1.8$  and 2.3. The spin characters of O, M and I show discontinuous jumps, which indicate 1<sup>st</sup>-order transitions in our approximation. The electron charge density hardly varies through the entire regime, and shows no sign of charge-driven reconstruction [22, 27].

The emergence of mode-switching is quite robust. The phases and phase transitions are qualitatively unaffected by including LL/spin mixing to higher LLs ( $n > 2$ ). Phases B and C occur over a very broad range of  $\tilde{w}$ , (Phase C exists at least up to  $\tilde{w} = 11$ ). Upon increasing the Zeeman coupling, the bulk phase boundary between the partially and fully polarized states moves lower in  $\tilde{E}_c$  and edge Phase C encroaches on edge Phase B. Furthermore, the lower boundary between Phase A and Phase B in Fig. 1(a) moves upwards. Reducing the range of the interaction by increasing  $q_{sc}\ell$  moves the phase boundaries of edge phases B and C towards larger  $\tilde{w}$ . Upon independently varying the strength of the direct ( $E_{cd}$ ) and exchange ( $E_{cx}$ ) terms, we find that mode-switching occurs in HF only if  $E_{cx} > 0.6E_{cd}$ , consistent with our claim that this is an exchange effect [22].

One limitation of HF is that the occupation  $n(k)$  of a single-particle state is either 0 or 1 (at  $T = 0$ ). To get beyond this limitation we investigated a class of variational states that do not conserve particle number and allow continuously varying  $0 \leq n(k) \leq 1$ . The simplest such state for the  $\nu = 1$  spin-polarized edge is  $|\psi\rangle = \prod_{k=1}^{N_s} (u_k + v_k e^{i\theta_k} c_k^\dagger)|0\rangle$ . Here  $u_k$ ,  $v_k$  are real numbers satisfying  $u_k^2 + v_k^2 = 1$ , and  $n(k) = v_k^2$ ,  $\theta_k$  is a set of phases chosen to minimize the translation-symmetry-breaking inherent in such states. This class includes HF states. For  $\nu = 3$  our variational state is [27]

$$|\psi\rangle = \prod_k (U_k + V_{0k} e^{i\theta_{0k}} c_{0k\uparrow}^\dagger + V_{1k} e^{i\theta_{1k}} c_{0k\downarrow}^\dagger c_{0k\uparrow}^\dagger + V_{2k} e^{i\theta_{2k}} c_{1k\uparrow}^\dagger c_{0k\uparrow}^\dagger + V_{3k} e^{i\theta_{3k}} c_{1k\uparrow}^\dagger c_{0k\downarrow}^\dagger c_{0k\uparrow}^\dagger)|0\rangle. \quad (6)$$

When  $E_{cx} < 0.4E_{cd}$  this ansatz does produce smoothly varying  $n(k)$  at  $\nu = 3$ , with the variational energy lower than the HF energy. However, upon increasing  $E_{cx}$  we recover the HF solution, lending further support to the validity of the latter (and to the transition being 1<sup>st</sup> order).

*Experimental signatures.* Before presenting transport signatures of the switching phenomenon [27], we note that whenever an edge changes from sharp to smooth, spin-mixed edge modes will undergo avoided

crossings with attendant spin rotations along the edge ( $x$ -direction) [28–30]. Further, the  $\nu = 2$  state becomes fully polarized at  $\tilde{E}_c \approx 2.13$  for the Coulomb interaction, in HF. If a QPC is tuned to be at a dimensionless two-terminal conductance  $g_2 = 2$ , the QPC region will be fully polarized in the regime where Phase C occurs, and unpolarized in the regime where Phase B occurs.

Our first “smoking gun” signature is in spin transport, as illustrated in Fig. 2. The system is tuned to be in the  $g_2 = 1$  or  $g_2 = 2$  conductance plateau, with the source

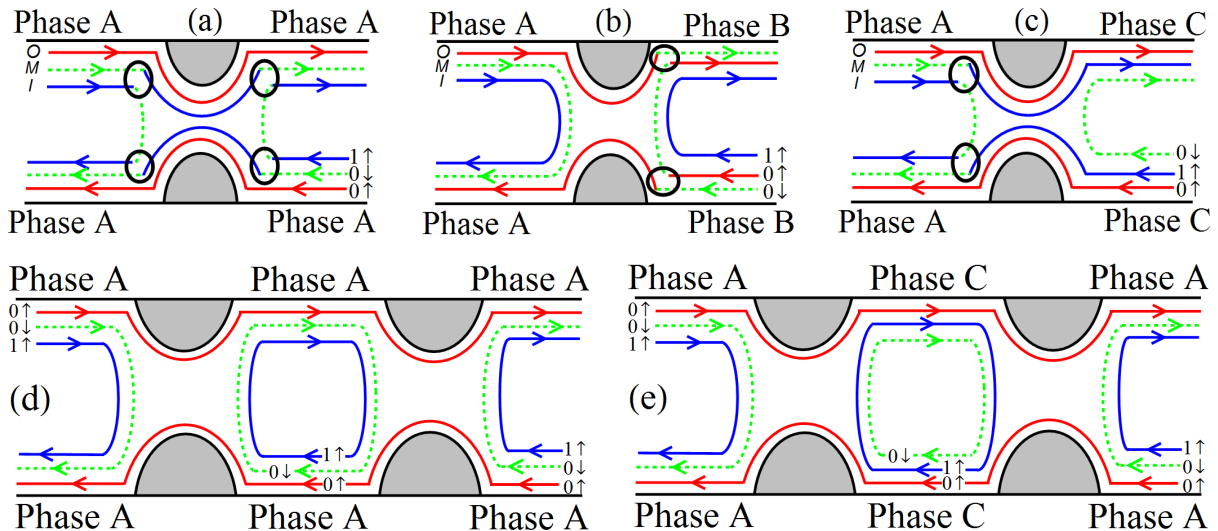


FIG. 2. (Color online) Experimental setups to show “smoking gun” signatures of mode switching. The source (drain) is always on the top left (right). Red solid lines depict the  $0\uparrow$  mode, green dashed lines the  $0\downarrow$  mode and blue solid lines the  $1\uparrow$  mode. The edges are labelled on the bottom right of each panel. Spin rotations in space are indicated by black circles.

(a),(b) and (c) Single QPC setups. (a) All the edges are in Phase A,  $g_2 = 2$ , and  $\tilde{E}_c > 2.13$ . The full polarization of the  $\nu = 2$  QPC region forces the M and I modes undergo a spin-rotation upon entering the QPC, and an inverse rotation upon exit. The incoming/outgoing current is spin unpolarized. (b) When the edges to the right of the QPC are in Phase B, the current at  $g_2 = 1$  reverses spin-polarization from  $\uparrow$  to  $\downarrow$  at the QPC. (c) When the edges to the right of the QPC are in Phase C, the current (from A to C) at  $g_2 = 2$  changes from spin-unpolarized to spin-polarized at the QPC.

(d) and (e) Two-QPC setups at  $g_2 = 1$ . (d) When the confining potential in the middle section is sharp on both the upper and lower edges (in Phase A), a high quality  $g_2 = 1$  plateau emerges. (e) When the confining potential in the middle section is smooth at both edges (in Phase C), disorder-induced degradation of the conductance plateau due to backscattering in the inter-QPC region is expected.

on the top left, in Fig. 2. Spin rotations in space are indicated by black circles on the figures, with the modes changing color (and changing from solid to dashed (i.e., from spin up to spin down) or vice versa). The current is carried by the channels O and M (Fig. 2(a)). For all edges sharp and  $\tilde{E}_c > 2.13$ , there is a nontrivial spin rotation of M as it enters the QPC region, but it rotates back upon exiting the QPC, so that the current in the drain (top right) remains unpolarized. However, when the right side is in Phase C, (Fig. 2(c)), the current in the drain is spin polarized  $\uparrow$ . In Fig. 2(b) we show a QPC tuned to  $g_2 = 1$  in the regime where Phase B occurs. Recall that Phase B has  $O=0\downarrow$ ,  $M=0\uparrow$  and  $I=1\uparrow$ . The source current (top left) is  $\uparrow$  but the drain current (top right) is  $\downarrow$ .

For our next signature, we consider the effect of static, non-magnetic disorder, which allows tunneling between neighboring chiral modes of the same spin. In Fig. 2(d) and 2(e), the region outside the two QPCs is in Phase A. We tune the system to the  $g_2 = 1$  plateau. If the inter-QPC region is in Phase A, the opposite spin polarizations of the two outer channels  $0\uparrow, 0\downarrow$  prevent disorder-induced tunneling, as shown in Fig. 2(d). On the other hand, when both the top and bottom edges of the inter-QPC region are in Phase C (Fig. 2(e)), the two outer channels have same spin and disorder-induced tunneling is

allowed on both the top and bottom edges. This leads to backscattering, and hence to a degradation of the quantization of the conductance plateau. Similar results hold for  $g_2 = 2$  with the inter-QPC region being either in Phase A (no disorder-induced degradation) or in Phase B (disorder-induced degradation) [27].

*Summary and discussion.* We have found spin-exchange driven edge phases and quantum phase transitions that take place at  $\nu = 3$  for low Zeeman energies. Our control parameters are the interaction strength  $\tilde{E}_c$  and the edge width  $\tilde{w}$ . We focus on  $\tilde{E}_c \lesssim 2.5$ : a partially polarized bulk state with the LLs  $0\uparrow$ ,  $0\downarrow$  and  $1\uparrow$  occupied. For small  $\tilde{w}$  (edge Phase A), the order of the edges follows the bulk order. However, as  $\tilde{w}$  becomes larger, we find two distinct edge mode-switched phases: For  $1.5 \lesssim \tilde{E}_c \lesssim 2.13$ , Phase B occurs with the edge ordering  $O=\text{outermost}=0\downarrow$ ,  $M=\text{middle}=0\uparrow$  and  $I=\text{innermost}=1\uparrow$ . For  $2.13 \lesssim \tilde{E}_c \lesssim 2.5$  Phase C occurs with the edge ordering  $O=0\uparrow$ ,  $M=1\uparrow$  and  $I=0\downarrow$ . Heuristically, these phases result from an exchange attraction between the like-spin edge modes. Employing approximate analytical methods (the spin unrestricted Hartree-Fock approximation, and minimization with respect to a particle non-conserving variational state) we find the transitions to be 1<sup>st</sup>-order. We stress that there is no significant charge

rearrangement associated with these transitions, putting spin-mode-switching in a qualitatively different category from the extensively investigated phenomena of charge-driven edge reconstruction. The crucial requirements for the switching transition to occur are: (i) A partially polarized bulk state. (ii) Moderate to strong interaction strength  $\bar{E}_c$ . (iii) A smooth edge. We have also provided experimental signatures of such transitions in charge and spin transport, relying on experimentally accessible setups with one or more quantum point contacts.

Our findings have diverse implications, e.g.: (i) Bulk  $\nu = 1$  supports charged skyrmions [31], while bulk  $\nu = 3$  does not [32, 33]. The  $\nu = 1$  spinful edge is known to be unstable to the formation of edge skyrmions [34]. Similar edge spin texture instabilities would likely arise in our  $\nu = 3$  system, especially in Phase C, with some similarities to charge-neutral bilayer graphene [35]. (ii) Our results should have direct analogues at  $\nu = 4$ , and more interestingly, in the QHE in graphene [36–38]. (iii) Our analysis should generalize to fractional quantum Hall states such as  $\nu = \frac{3}{7}$ , which is the composite fermion analog [39] of the  $\nu = 3$  state.

GM thanks Sid Parameswaran for illuminating discussions, and acknowledges the Aspen Center for Physics (NSF Grant No. 1066293) for its hospitality, the US-Israel BSF (grants 2012120 and 2016130) and NSF-DMR 1306897 for support. YG thanks Dmitry G. Polyakov for useful discussions, and acknowledges ISF (grant 1349/14), the DFG (grants RO 2247/8-1, CRC 183), the IMOS Israel-Russia program, and Minerva for support.

- 
- [1] B. I. Halperin, Phys. Rev. B **25**, 2185 (1982).  
 [2] X.-G. Wen, Phys. Rev. Lett. **64**, 2206 (1990).  
 [3] D. B. Chklovskii, B. I. Shklovskii, and L. I. Glazman, Phys. Rev. B **46**, 4026 (1992).  
 [4] J. Dempsey, B. Y. Gelfand, and B. I. Halperin, Phys. Rev. Lett. **70**, 3639 (1993).  
 [5] C. de C. Chamon and X.-G. Wen, Phys. Rev. B **49**, 8227 (1994).  
 [6] A. H. MacDonald, Phys. Rev. Lett. **64**, 220 (1990); M. D. Johnson and A. H. MacDonald, Phys. Rev. Lett. **67**, 2060 (1991); A. H. MacDonald, S. R. Eric Yang, and M. D. Johnson, Aust. J. Phys **46**, 345 (1993).  
 [7] Y. Meir, Phys. Rev. Lett. **72**, 2624 (1994).  
 [8] C. L. Kane, Matthew P. A. Fisher, and J. Polchinski, Phys. Rev. Lett. **72**, 4129 (1994).  
 [9] C. L. Kane and Matthew P. A. Fisher, Phys. Rev. Lett. **76**, 3192 (1996).  
 [10] O. Klein, C. de C. Chamon, D. Tang, D. M. Abusch-Magder, U. Meirav, X.-G. Wen, M. A. Kastner, and S. J. Wind, Phys. Rev. Lett. **74**, 785 (1995).  
 [11] N. B. Zhitenev, M. Brodsky, R. C. Ashoori, and M. R. Melloch, Phys. Rev. Lett. **77**, 1833 (1996).  
 [12] V. Venkatachalam, S. Hart, L. Pfeiffer, K. West, and A. Yacoby, Nature Phys. **8**, 676 (2012).  
 [13] A. Grivnin, H. Inoue, Y. Ronen, Y. Baum, M. Heiblum, V. Umansky, and D. Mahalu, Phys. Rev. Lett. **113**, 266803 (2014).  
 [14] R. Sabo, I. Gurman, A. Rosenblatt, F. Lafont, D. Banitt, J. Park, M. Heiblum, Y. Gefen, V. Umansky, and D. Mahalu, Nature Phys. **13**, 491 (2017).  
 [15] X. Wan, K. Yang, and E. H. Rezayi, Phys. Rev. Lett. **88**, 056802 (2002).  
 [16] K. Yang, Phys. Rev. Lett. **91**, 036802 (2003).  
 [17] Y. Zhang, Z.-X. Hu, and K. Yang, Phys. Rev. B **88**, 205128 (2013).  
 [18] Y. Barlas, Y. N. Joglekar, and K. Yang, Phys. Rev. B **83**, 205307 (2011).  
 [19] Y. Zhang and K. Yang, Phys. Rev. B **87**, 125140 (2013).  
 [20] J. Wang, Y. Meir, and Y. Gefen, Phys. Rev. Lett. **111**, 246803 (2013).  
 [21] J. Wang, Y. Meir, and Y. Gefen, Phys. Rev. Lett. **118**, 046801 (2017).  
 [22] Coulomb interactions have both direct and exchange components, so there can be confusion about what is meant by “charge” versus “exchange” effects. Our working definition is that when a reorganization of the charge density occurs as a consequence of an edge reconstruction it is essentially a “charge” effect, while any reconstruction without such a reorganization of charge density is essentially an “exchange” effect.  
 [23] R. E. Prange and S. M. Girvin, The Quantum Hall Effect, Springer-Verlag New York (1990).  
 [24] T. Jungwirth and A. H. MacDonald, Phys. Rev. B **63**, 035305 (2000).  
 [25] J. T. Chalker, D. G. Polyakov, F. Evers, A. D. Mirlin, and P. Wolfe, Phys. Rev. B **66**, 161317(R) (2002).  
 [26] E. H. Rezayi, T. Jungwirth, A. H. MacDonald, and F. D. M. Haldane, Phys. Rev. B **67**, 201305 (2003).  
 [27] Further details are presented in the Supplemental Material.  
 [28] Our work so far has focused on translation invariant states along the edge. In the situations we consider for experimental signatures, the slope of  $V_{\text{edge}}$  changes along the edge. We assume that as long as the changes occur over a scale long compared to  $\ell$  our analysis remains valid. We also assume that in this region, there is a mechanism which allows the spin to relax to its equilibrium value.  
 [29] D. G. Polyakov, Phys. Rev. B **53**, 15777 (1996).  
 [30] D. I. Golosov, I. Shlimak, A. Butenko, K.-J. Friedland, and S. V. Kravchenko, Phys. Rev. B **88**, 155313 (2013).  
 [31] S. L. Sondhi, A. Karlhede, S. A. Kivelson, and E. H. Rezayi, Phys. Rev. B **47**, 16419 (1993).  
 [32] J. K. Jain and X. G. Wu, Phys. Rev. B **49**, 5085(R) (1994).  
 [33] X. G. Wu and S. L. Sondhi, Phys. Rev. B **51**, 14725 (1995).  
 [34] A. Karlhede, S. A. Kivelson, K. Lejnell, and S. L. Sondhi, Phys. Rev. Lett. **77**, 2061 (1996).  
 [35] D. A. Abanin, S. A. Parameswaran, and S. L. Sondhi, Phys. Rev. Lett. **103**, 076802 (2009).  
 [36] D. A. Abanin, P. A. Lee, and L. S. Levitov, Phys. Rev. Lett. **96**, 176803 (2006).  
 [37] L. Brey and H. A. Fertig, Phys. Rev. B **73**, 195408 (2006).  
 [38] H. A. Fertig and L. Brey, Phys. Rev. Lett. **97**, 116805 (2006).  
 [39] J. K. Jain, Phys. Rev. Lett. **63**, 199 (1989); Phys. Rev. B **41**, 7653 (1990); *Science* **266**, 1199 (1994).

# Supplementary material for Spin Mode-Switching at the Edge of a Quantum Hall System

Udit Khanna,<sup>1,2</sup> Ganpathy Murthy,<sup>3</sup> Sumathi Rao,<sup>1,2</sup> and Yuval Gefen<sup>4</sup>

<sup>1</sup>*Harish-Chandra Research Institute, Chhatnag Road, Jhansi, Allahabad 211019, India*

<sup>2</sup>*Homi Bhabha National Institute, Training School Complex, Anushaktinagar, Mumbai, Maharashtra 400085, India*

<sup>3</sup>*Department of Physics and Astronomy, University of Kentucky, Lexington KY 40506-0055, USA*

<sup>4</sup>*Department of Condensed Matter Physics, Weizmann Institute, 76100 Rehovot, Israel*

PACS numbers: 73.21.-b, 73.22.Gk, 73.43.Lp, 72.80.Vp

In this set of supplemental materials we provide the details of our theoretical calculations. In Section I we establish our notation and present the basic setup. Next, in Section II we present the Hartree-Fock (HF) approximation both in the bulk and near the edge. In particular we show the first order bulk transition of the  $\nu = 3$  quantum Hall state from partially polarized to fully polarized as the interaction scale increases. In Section II we also present our edge calculation, where we show the difference between spin-unrestricted HF and spin-conserving HF, focusing on the region near the spin-mode-switching transition. We follow this in Section III with a presentation of the number non-conserving variational states which go beyond HF. We show an illustrative example for  $\nu = 1$  where we see a smooth variation of the occupation number and then proceed to the details of the actual case of interest  $\nu = 3$ . Finally, in Section IV we provide additional transport scenarios, beyond those presented in the main text, which can be used to test for spin-mode-switching.

## I. BASIC SETUP

Consider the integer quantum Hall state on a cylinder. Assuming  $x$  to be the periodic direction, the wavefunction for single-particle states in Landau gauge  $eA_x = -y/\ell^2$ ,  $eA_y = 0$ , is

$$\Phi_{nk}(x, y) = \frac{e^{ikx}}{\sqrt{L_x}} \frac{e^{-\frac{(y-k\ell^2)^2}{2\ell^2}}}{\sqrt{2^n n! \ell \sqrt{\pi}}} H_n \left( \frac{y - k\ell^2}{\ell} \right) \quad (S1)$$

where  $n$  is the Landau level index,  $k$  is the guiding center index localized about  $Y = k\ell^2$ ,  $\ell = \sqrt{\frac{\hbar}{eB}}$  is the magnetic length and  $H_n$  is the  $n^{\text{th}}$  Hermite polynomial. The Hamiltonian of the system consists of 3 terms: the cyclotron term  $H_c$ , electron-background attraction  $H_{bg}$ , and electron-electron repulsion  $H_{ee}$ . Using  $c_{nks}$  as the destruction operator for single-particle state  $\Phi_{nk}$  and spin

$s = \uparrow, \downarrow$ , these are

$$H_c = \sum_{nks} n\hbar\omega_c c_{nks}^\dagger c_{nks} \quad (S2)$$

$$H_{bg} = -\frac{1}{A} \sum_{\vec{q}} v(\vec{q}) \rho_b(-\vec{q}) \rho_e(\vec{q}) \quad (S3)$$

$$H_{ee} = \frac{1}{2A} \sum_{\vec{q}} v(\vec{q}) : \rho_e(\vec{q}) \rho_e(-\vec{q}) :, \quad (S4)$$

where  $\omega_c = \frac{eB}{m}$  is the cyclotron gap,  $A$  is the area of the sample,  $v(\vec{q})$  is the Fourier transform of the electron-electron interaction,  $\rho_b(\vec{q})$  is the background density, and  $\rho_e(\vec{q})$  is the electron density operator, which is

$$\rho_e(\vec{q}) = \sum_{\{n\}ks} e^{-iq_y(k + \frac{qx}{2})\ell^2} \rho_{n_1 n_2}(\vec{q}) c_{n_1 ks}^\dagger c_{n_2 k+qx s} \quad (S5)$$

where  $\{n\}$  denotes the tuple  $(n_1, n_2, \dots)$ . For  $n_1 \geq n_2$  the matrix element  $\rho_{n_1 n_2}$  is,

$$\rho_{n_1 n_2}(\vec{q}) = \sqrt{\frac{n_2!}{n_1!}} \left( \frac{q\ell e^{-i\theta_q}}{\sqrt{2}} \right)^{(n_1 - n_2)} L_{n_2}^{n_1 - n_2} \left( \frac{q^2 \ell^2}{2} \right) e^{-\frac{q^2 \ell^2}{4}}, \quad (S6)$$

where  $L_n^m$  is the associated Laguerre polynomial and  $\rho_{n_2 n_1}(\vec{q}) = [\rho_{n_1 n_2}(-\vec{q})]^*$ .

The background charge is assumed to be uniformly distributed in the  $x$  direction. Then  $\rho_b(\vec{q}) = \delta_{q_x, 0} \rho_b(q_y)$  and therefore the background term is,

$$H_{bg} = -\frac{1}{A} \sum_{\{n\}ks} \sum_{\vec{q}} v(\vec{q}) \Delta_{bg}(\{n\}, k, \vec{q}) c_{n_1 ks}^\dagger c_{n_2 ks}, \quad (S7)$$

where the background potential is

$$\Delta_{bg}(\{n\}, k, \vec{q}) = \delta_{q_x, 0} \rho_b(-q_y) e^{-iq_y k} \rho_{n_1 n_2}(\vec{q}) \quad (S8)$$

Here, the edge is modelled with a background charge density that falls linearly from the bulk value  $\frac{\nu e}{2\pi\ell^2}$  to 0 over a width of  $W$  around  $y = 0$  [1, 2] (Fig. S1).

$$\rho_b(\vec{r}) = \begin{cases} \frac{\nu e}{2\pi\ell^2} & \text{for } y \leq -\frac{W}{2} \\ \frac{\nu e}{2\pi\ell^2} \frac{W - 2y}{2W} & \text{for } -\frac{W}{2} \leq y \leq \frac{W}{2} \\ 0 & \text{for } \frac{W}{2} \leq y \end{cases} \quad (S9)$$

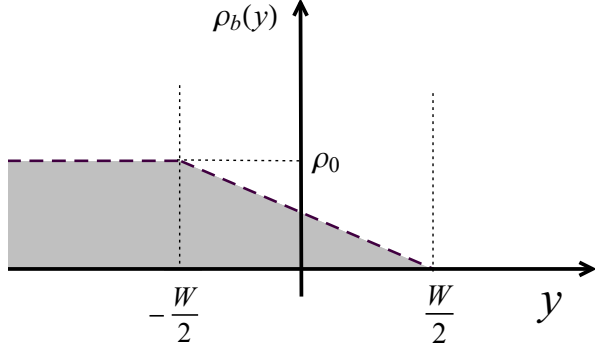


FIG. S1. (Color online) The background density falls linearly from  $\rho_0 = \frac{\nu e}{2\pi\ell^2}$  to 0 in a distance  $W$ .

## II. HARTREE FOCK CALCULATION

In the Hartree Fock (HF) approximation, the interaction term  $H_{ee}$  is decoupled by taking all possible averages and replaced by a one body mean-field Hamiltonian  $H_{MF}$ . Under the assumption that the state has translation invariance in the  $x$ -direction, the averages have the form,

$$\langle c_{n_1 k_1 s_1}^\dagger c_{n_2 k_2 s_2} \rangle = \delta_{k_1 k_2} \Delta_{n_1 n_2; s_1 s_2}(k), \quad (\text{S10})$$

and thus

$$H_{MF} = \frac{1}{A} \sum_{\{n,s\}} \sum_{k\vec{q}} v(\vec{q}) \begin{bmatrix} V_H(\{n,s\}, k, \vec{q}) \\ -V_F(\{n,s\}, k, \vec{q}) \end{bmatrix} c_{n_1 k s_1}^\dagger c_{n_2 k s_2}$$

$$V_H(\{n,s\}, k_1, \vec{q}) = \sum_{\{m\}k_2\sigma} \begin{bmatrix} \delta_{s_1 s_2} \delta_{q_x, 0} e^{-iq_y(k_1 - k_2)\ell^2} \\ \times \Delta_{m_1 m_2; \sigma\sigma}(k_2) \\ \times \rho_{n_1 n_2}(\vec{q}) \rho_{m_1 m_2}(-\vec{q}) \end{bmatrix} \quad (\text{S11})$$

$$V_F(\{n,s\}, k, \vec{q}) = \sum_{\{m\}} \begin{bmatrix} \Delta_{m_1 m_2; s_2 s_1}(k + q_x) \\ \times \rho_{n_1 n_2}(\vec{q}) \rho_{m_1 n_2}(-\vec{q}) \end{bmatrix}, \quad (\text{S12})$$

where the Hartree and Fock potentials ( $V_{H/F}$ ) have to be computed self-consistently. The Hartree potential arises from the classical density-density interaction and therefore is same for both spin states. The spin-dependent Fock potential arises due to the exchange of electrons and promotes ferromagnetic behaviour.

**Bulk Solution:** In the bulk, the electron charge density is fully translation invariant, implying that the matrix elements  $\Delta_{n_1 n_2; s_1 s_2}$  are independent of the guiding center label  $k$ . In the presence of an infinitesimal Zeeman field, the spins of all the single-particle states will be either parallel or antiparallel to the quantization axis, implying that  $\Delta$  is diagonal in spin labels. Furthermore, no LL-mixing occurs in translation invariant HF states.

Therefore  $\Delta$  reduces to a diagonal matrix in both spin and Landau level indices, in which the diagonal elements are the occupations of the single-particle levels. Thus, the HF potentials depend only on the occupations of the single-particle levels. In the bulk, the Hartree potential cancels the background potential exactly due to charge neutrality. The Fock potentials reduce to

$$V_F(n, s, \vec{q}) = \sum_m n_f(m; s) \rho_{nm}(\vec{q}) \rho_{mn}(-\vec{q}).$$

The energy (per particle) of a translation-invariant bulk HF state with occupations  $n_f(m; s)$  is

$$E[n_f(m; s)] = \sum_{\{m\}, s} \frac{n_f(m_1; s)}{\nu} \begin{bmatrix} \delta_{m_1, m_2} m_1 \hbar\omega_c \\ -E_{ex}(m_1, m_2) n_f(m_2; s) \end{bmatrix},$$

where the exchange energy is

$$E_{ex}(m_1, m_2) = \frac{1}{2} \int \frac{d^2 q}{(2\pi)^2} v(\vec{q}) \rho_{m_1 m_2}(\vec{q}) \rho_{m_2 m_1}(-\vec{q}).$$

These integrals can be calculated analytically for certain special forms of  $v(\vec{q})$ , such as the Coulomb interaction. At zero temperature, the occupation of a single-particle level is either 1 or 0. Given the occupations of a HF state, its energy can be calculated easily. We drop the Hartree term in the bulk, since it contributes equally to all states.

At filling factor  $\nu = 3$ , the two possible translation-invariant ground states are the partially polarized state  $|\psi_1\rangle = |0\uparrow, 0\downarrow, 1\uparrow\rangle$  and the fully polarized state  $|\psi_2\rangle = |0\uparrow, 1\uparrow, 2\uparrow\rangle$ . We assume a screened Coulomb interaction of the form

$$v(\vec{q}) = \frac{2\pi E_c}{q + q_{sc}},$$

for which the energy can be expressed in terms of the Error function.  $E_c = \tilde{E}_c \hbar\omega_c = \frac{e^2}{4\pi\epsilon\ell}$  is the interaction scale as defined in the main text. For a long range Coulomb interaction ( $q_{sc} = 0$ ), the expression simplifies to -

$$E[|\psi_1\rangle] = \frac{1}{3} \hbar\omega_c - \frac{5}{8} E_c \sqrt{\frac{\pi}{2}}$$

$$E[|\psi_2\rangle] = \hbar\omega_c - \frac{107}{128} E_c \sqrt{\frac{\pi}{2}}$$

Comparing the two energies, we see that there is a 1<sup>st</sup> order [3, 4] bulk transition from  $|\psi_1\rangle$  to  $|\psi_2\rangle$  at  $\tilde{E}_c \approx 2.52$ . At finite values of  $q_{sc}$ , the exchange interaction is weaker and the transition occurs at a larger value of  $\tilde{E}_c$ . In the numerical calculations to follow, we have used  $q_{sc}\ell = 0.01$  for which the transition occurs at  $\tilde{E}_c \approx 2.53$ . Similar considerations lead to a bulk 1<sup>st</sup> order transition of the  $\nu = 2$  state from unpolarized to fully polarized at  $\tilde{E}_c = 2.13$ .

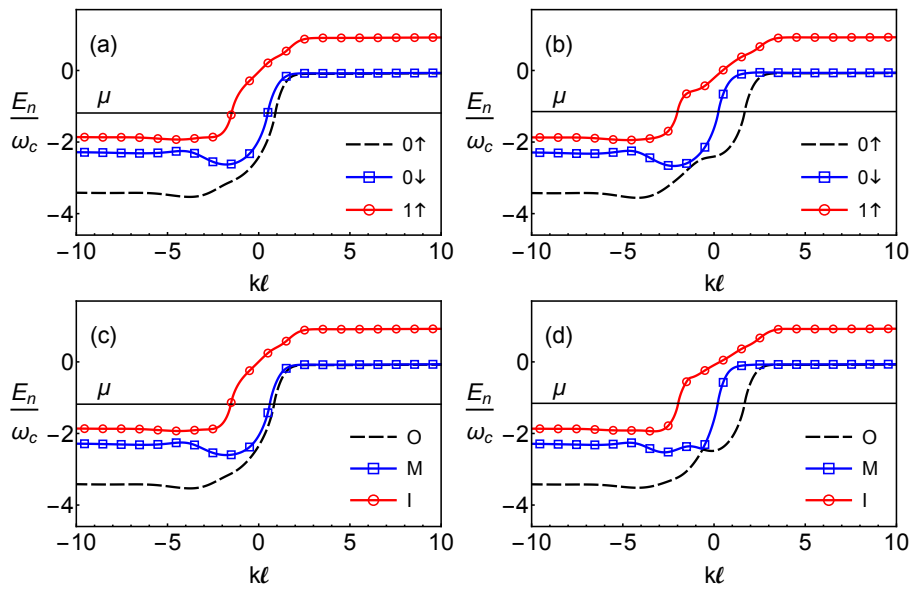


FIG. S2. (Color online) Comparison of the self-consistent single particle energy level dispersion in RHF (spin-restricted HF, cf. Eq. S10 and S14) and UHF (spin-unrestricted HF, i.e. without the restriction in Eq. S14) at  $\tilde{E}_c = 1.8$ . In RHF we can label an energy dispersion with the LL-index it had in the bulk and its spin. In UHF, however, spin is not conserved, so we label the modes in the order they appear at the edge from outside in, as  $i = O$  (outermost),  $M$  (middle), and  $I$  (innermost). (a) Self-consistent single-particle energy dispersions vs.  $k\ell$  in RHF for  $W = 2.0\ell$  (Phase A). The order of the edges, from outermost to innermost, is the same as the bulk order of energies from lowest to highest. (b) Single-particle energy dispersions vs.  $k\ell$  for  $W = 4.0\ell$  in RHF. The true ground state is Phase B, but RHF is unable to reach the true ground state, so the figure shows the dispersions in a metastable Phase A. (c) Single-particle energy dispersions vs.  $k\ell$  for  $W = 2.0\ell$  in UHF. Since the true ground state is that of Phase A, almost no spin-rotations are required, and the dispersions are very close to those of RHF. (d) Single-particle energy dispersions vs.  $k\ell$  at  $W = 4.0\ell$  in UHF. Now the system is in Phase B. Note that the apparent touching of the  $O$  and  $M$  modes near  $k\ell = 0$  is actually an avoided crossing where the spin character of the single particle levels changes (see Fig. S3(b) below).

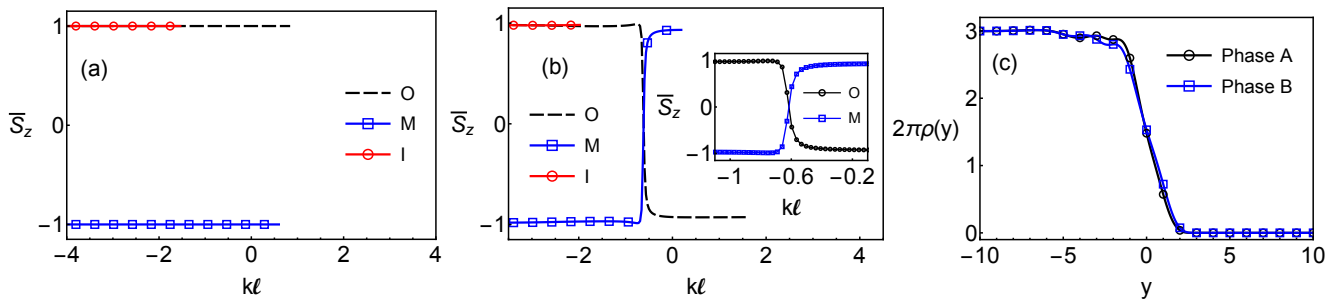


FIG. S3. (Color online) (a)  $\bar{S}_z(i, k)$  of single particle energy levels in UHF vs.  $k\ell$  at  $\tilde{E}_c = 1.8$  and  $W = 2.0\ell$  (Phase A). There are no spin-rotations. (b)  $\bar{S}_z(i, k)$  in UHF vs.  $k\ell$  at  $\tilde{E}_c = 1.8$  and  $W = 4.0\ell$  (Phase B). Note that  $\bar{S}_z(i, k)$  for  $i = O$  and  $M$  vary continuously near  $k\ell = 0$ , precisely where the corresponding energy dispersions (Fig. S2(d)) appear to touch. The inset makes the smooth variation of  $\bar{S}_z(i, k)$  unambiguous. This is evidence that the apparent touching is actually an avoided crossing. At an actual crossing,  $\bar{S}_z(i, k)$  would have changed abruptly. (c) The average of the electronic density  $\rho(y)$  vs.  $y$  just before and after the mode-switching transition in Phase A (at  $W = 3.25\ell$ ,  $\tilde{E}_c = 1.8$ ) and in Phase B (at  $W = 3.75\ell$ ,  $\tilde{E}_c = 1.8$ ). It is seen that there is very little variation of the electron charge density across the transition, which is the basis of our conclusion that the mode-switching transition is not driven by charge effects.

**Edge Solution:** We will assume translation-invariance along the edge ( $x$ -direction) so that equation S10 holds and  $\Delta_{n_1 n_2; s_1 s_2}(k)$  remains diagonal in  $k$ . However, close to the edge  $\Delta$  does depend on  $k$ . Fur-

thermore, Landau levels with different  $n$  will generically hybridize in order to lower the overall energy, leading to LL-mixing. We compute the ground state in both the (spin-)restricted HF (RHF), which assumes that  $\Delta$  remains diagonal in spin indices, and in (spin-)unrestricted HF (UHF) which relaxes this assumption and allows spin-

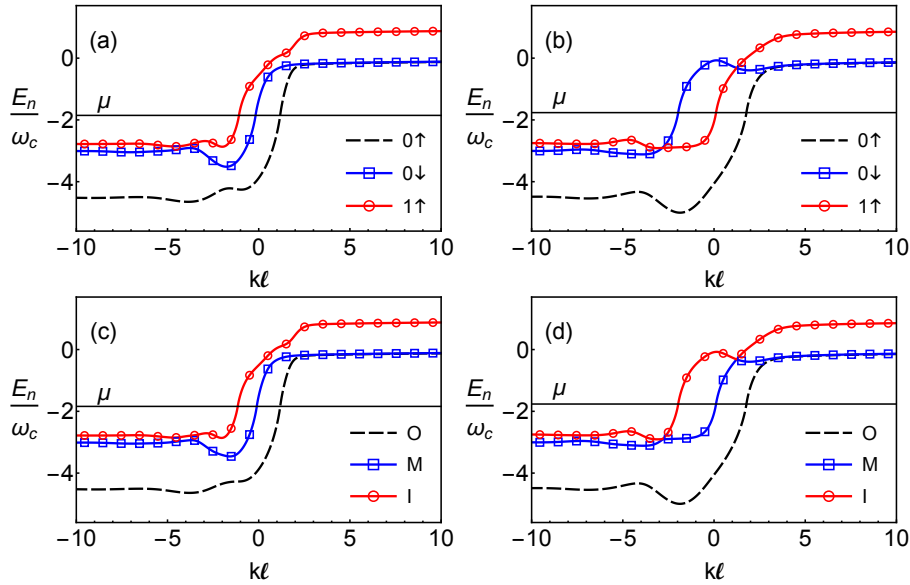


FIG. S4. (Color online) Comparison of the self-consistent energy dispersions in RHF and UHF at  $\tilde{E}_c = 2.3$ . (a) Energy dispersions vs.  $kl$  at  $W = 2.0\ell$  in RHF. As always in Phase A, there are no level crossings. (b) Energy dispersions vs.  $kl$  at  $W = 4.5\ell$  in RHF (Phase C). RHF is able to access Phase C, and one sees the 0 $\downarrow$  and 1 $\uparrow$  levels cross below  $\mu$ , so that the ordering at the edge is, from the outermost in, 0 $\uparrow$ , 1 $\uparrow$ , and 0 $\downarrow$ . (c) Energy dispersions vs.  $kl$  at  $W = 2.0\ell$  in UHF (Phase A). There are no level crossings. (d) Energy dispersions vs.  $kl$  at  $W = 4.5\ell$  in UHF (Phase C). Note that the apparent touching of M and I near  $kl = -3$  is actually an avoided crossing, as evidenced by  $\bar{S}_z(i, k)$  (see Fig. S5(b) below).

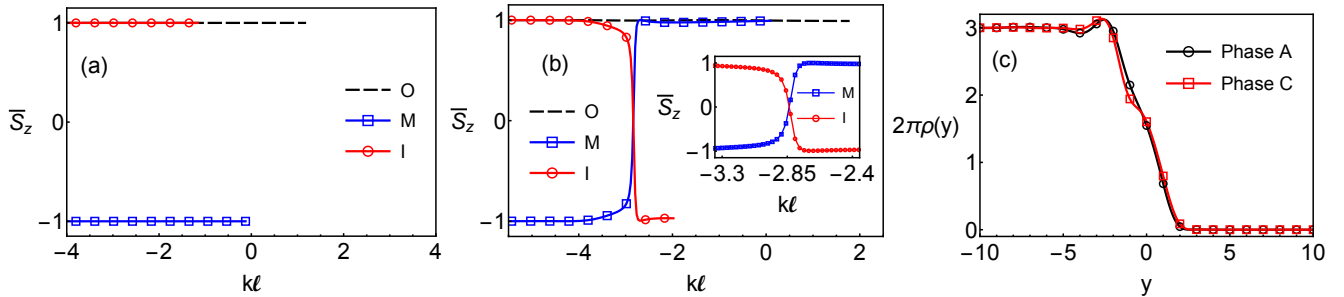


FIG. S5. (Color online) (a) and (b)  $\bar{S}_z(i, k)$  vs.  $kl$  of single particle energy levels at  $\tilde{E}_c = 2.3$  in UHF. (a) At  $W = 2.0\ell$  the system is in Phase A, and  $\bar{S}_z(i, k)$  are independent of  $k$ . (b) At  $W = 4.5\ell$  the system is in Phase C. Note that the spin character in (b) changes smoothly near the guiding centers where the energy levels M and I show an avoided crossing (Fig. S4(d)). The inset makes this smooth variation clear. (c) The average of the electronic charge density  $\rho(y)$  vs.  $y$  just before and after the mode-switching transition in Phase A (at  $W = 4.0\ell$ ,  $\tilde{E}_c = 2.3$ ) and in Phase C (at  $W = 4.5\ell$ ,  $\tilde{E}_c = 2.3$ ). Once again, we see that there is hardly any variation across the transition, supporting our conclusion that the spin-mode-switching transition is not driven by charge effects, but rather primarily by spin-exchange.

mixing. We describe below the numerical method used to compute the ground state and then compare the results at the edge for restricted and unrestricted HF.

After the HF averages are taken, the HF Hamiltonian becomes diagonal in the guiding center label  $k$ . We choose  $L_x = 200\ell$ , which leads to roughly 32 guiding centers per magnetic length  $\ell$ . We truncate the Hilbert space and restrict the number of Landau levels (per spin) to  $N$  (where  $N = 3$  for all our results). Two kinds of  $k$  labels enter the calculation: “frozen” and active. The frozen  $k$  labels occur in the range  $-35 < kl < -20$ . The occupations in these values of  $k$  are fixed to be those of the

partially polarized bulk  $\nu = 3$  state throughout the calculation. The active levels occur for  $-20 \leq kl \leq 20$ , and for these levels we allow all values of  $\Delta$  consistent with translation symmetry along the edge. In computing the  $V_{H/F}$  potentials for the active states it is important to include the contribution of the frozen states. The presence of these frozen states serves to impose the proper bulk boundary condition for the active states.

The self-consistent ground state can then be found by the following iterative procedure. For a given set of matrix elements  $\Delta_{n_1 n_2; s_1 s_2}(k)$  (such that the total number of electrons is  $N_e$  consistent with charge neutrality, at

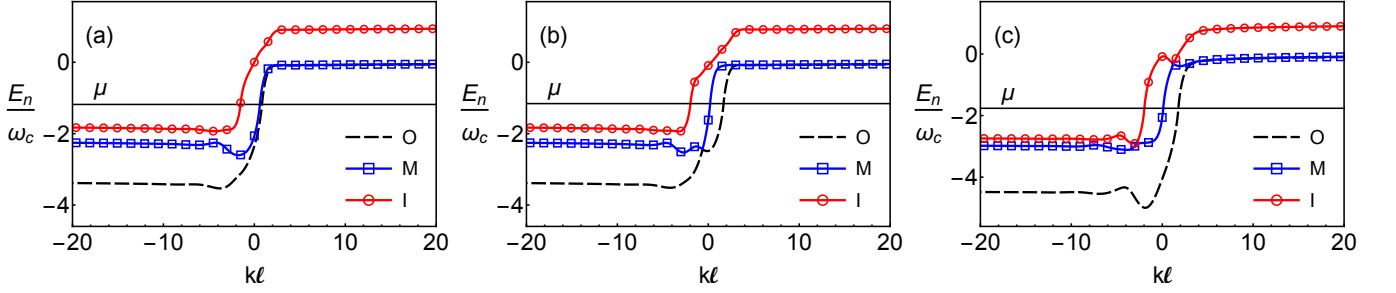


FIG. S6. (Color online) The self-consistent single particle energy level dispersion in UHF (spin-unrestricted HF, i.e. without the restriction in Eq. S14) in the full range of active guiding centers. The dispersion neatly converges to the expected value on both the boundaries for all the values of  $W$  considered in this work. (a) At  $W = 2.0\ell$ ,  $\tilde{E}_c = 1.8$  (Phase A). (b) At  $W = 4.0\ell$ ,  $\tilde{E}_c = 1.8$  (Phase B). (c) At  $W = 4.75\ell$ ,  $\tilde{E}_c = 2.3$  (Phase C).

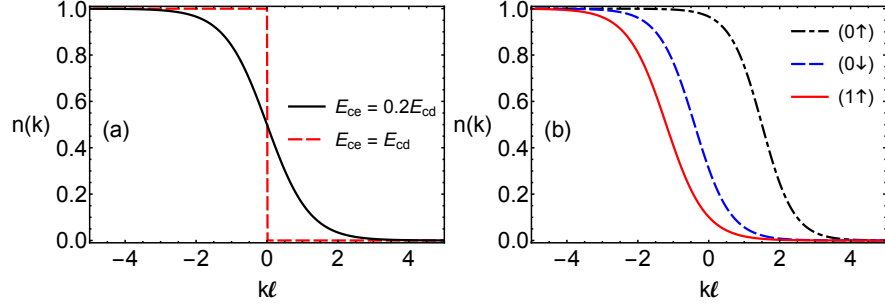


FIG. S7. (Color online) Ground state occupations in the variational state (a) at  $\nu = 1$  and (b) at  $\nu = 3$  (at  $E_{cx} = 0.2E_{cd}$ ). At  $E_{cx} = E_{cd}$ , the variational ansatz reproduces the HF state.

temperature  $T$ ), the HF potentials are computed through equations (S11) and (S12). Diagonalizing the  $2N \times 2N$  Hamiltonian at each guiding center gives the new single-particle states with energy  $\epsilon_{nks}$ . Next, the new chemical potential is computed by imposing the charge neutrality condition

$$\sum_{n,k,s} n_f(\epsilon_{nks}, \mu, T) = N_e, \quad (\text{S13})$$

where  $n_f(\epsilon, \mu, T) = 1/(e^{(\epsilon-\mu)/T} + 1)$  is the Fermi-Dirac distribution. This chemical potential is then used to compute the new matrix elements  $\Delta_{n_1 n_2; s_1 s_2}(k)$ . The cycle is repeated until self-consistency is achieved. In order to remove any dependence on the initial averages, the self-consistent solution is used as the seed for a new round of iterations in which the temperature is gradually increased and then decreased to zero.

In RHF, we assume

$$\Delta_{n_1 n_2; s_1 s_2}(k) = \delta_{s_1 s_2} \Delta_{n_1 n_2}(k, s_1). \quad (\text{S14})$$

Since spin is conserved in this approximation, we can label the final set of hybridized single-particle levels by spin. We use the non-interacting ground state as the starting seed for the iteration in this case. The self-consistent single-particle energy levels vs.  $k\ell$  at  $\tilde{E}_c = 1.8$  and two different values of  $W$  are shown in Fig. S2(a),(b).

Note that at  $\tilde{E}_c = 1.8$  (Fig. S2(a) and (b)) the order of the levels, from the outermost in, at the chemical potential  $\mu$  follows the bulk order or increasing energies. This is expected in Phase A, but is unexpected in Phase B. The reason for this result is that RHF is not able to find Phase B, so the RHF result depicts a metastable version of Phase A.

Now we turn to Fig. S4(a),(b) where we show the RHF results at  $\tilde{E}_c = 2.3$  for two different values of  $W$ . Once again, at  $W = 2\ell$  (Fig. S4(a)) we are in Phase A, and no level crossings are expected, and indeed none are seen. However, at  $W = 4.5\ell$  (Fig. S4(b)) there is a crossing of the  $0\downarrow$  and  $1\uparrow$  levels below  $\mu$ . This leads to the order of the edge modes being, from the outside in,  $0\uparrow$ ,  $1\uparrow$  and  $0\downarrow$ , thus showing a spin-mode-switching transition from phase A to C. In the absence of spin-mixing, the  $0\downarrow$  and  $1\uparrow$  levels can be degenerate, and as shown in Fig. S4(b), cross each other below and/or above the chemical potential.

Now we allow spin-mixing to occur in UHF. Operationally, we generate a spin-mixed seed by rotating the spins of the various single-particle levels in the RHF ground state in a small region close to  $k\ell = 0$ . The single-particle levels can no longer be labelled by spin, so we index them by  $i = O$  (outermost), M (middle), and I (innermost). The energy level dispersions vs.  $k$  for  $\tilde{E}_c = 1.8$  for two values of  $W$  are shown in Fig. S2(c),(d), and for

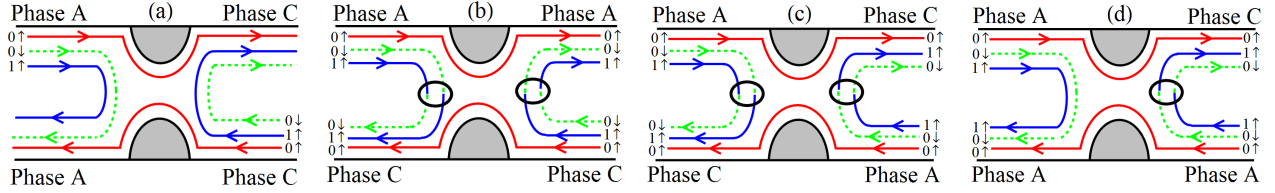


FIG. S8. (Color online) A single QPC tuned at the  $g_2 = 1$  plateau, connecting regions with different confining potentials. Here  $\tilde{E}_c > 2.13$  and hence the smooth edges are in Phase C. Spin rotations along the edge take place in the regions marked by black circles. The red (solid), green (dashed) and blue (solid) lines denote the  $(0\uparrow)$ ,  $(0\downarrow)$  and  $(1\uparrow)$  modes respectively. Disorder-induced tunneling between neighbouring same-spin voltage biased edge modes is implied. (a,b) If the source is at the top left, neighboring modes in Phase A are unable to tunnel into each other, being of opposite spin. Thus, no backscattering is expected. However, if the source is at the bottom right in Phase C, disorder induced tunneling can degrade the current, and reduce the quality of the conductance plateau. Thus, the left-right symmetry of the conductance plateau is broken. (c,d) Regardless of whether the source is at the top right or the bottom left, the source current is always in Phase A, which does not allow disorder-induced tunneling between neighboring modes. Thus, the left-right symmetry of the conductance plateau is not broken.

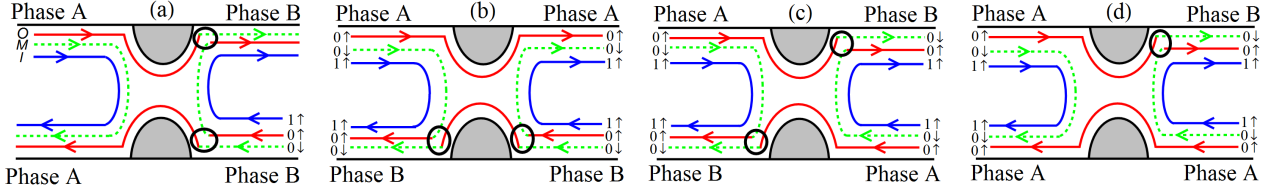


FIG. S9. (Color online) A single QPC tuned at the  $g_2 = 1$  plateau, connecting regions with different confining potentials. Here  $\tilde{E}_c < 2.13$ , hence the smooth edges are in Phase B. We employ the same notation as in Fig. S8. It is clear that in both Phases A and B, the two outer edges are of opposite spin. Therefore, disorder-induced tunneling is ineffective in degrading the conductance plateau at  $g_2 = 1$ , regardless of the locations of the source and drain.

$\tilde{E}_c = 2.3$  for two values of  $W$  are shown in S4(c),(d).

As in the main paper, to elucidate the physics of the spin-mode-switched phases, we compute  $\bar{S}_z(i, k)$ , the average of the operator  $S_z$  in the single-particle state labelled by  $i = O, M, I$ , at position  $kl$ . The importance of  $\bar{S}_z(i, k)$  is that its value at the position where it crosses the chemical potential,  $\bar{S}_{z\mu}(i)$ , determines the spin of the chiral edge mode.  $\bar{S}_z(i, k)$  vs.  $kl$  for occupied levels  $i$  are shown in Fig. S3(a),(b) and S5(a),(b), corresponding to the level dispersions of Fig. S2(c),(d) and S4(c),(d) respectively.

As seen in Fig. S3(a) and S5(a), in Phase A ( $W = 2.0\ell$ ),  $\bar{S}_z(i, k)$  are almost independent of  $k$ . In particular, at the point where the single-particle levels cross the chemical potential, the innermost (I) and outermost (O) levels have  $\bar{S}_z \approx 1$  while the middle level (M) has  $\bar{S}_z \approx -1$ . Fig. S3(b) and S5(b) show the  $\bar{S}_z$  after the mode-switching transition in Phase B ( $W = 4.0\ell$ ) and C ( $W = 4.5\ell$ ) respectively. Clearly, the  $\bar{S}_z(i, k)$  of two of the single particle levels (O & M in Phase B and I & M in Phase C) vary smoothly as they go through the avoided crossing. The insets show an expanded view near the location where most of the changes in  $\bar{S}_z(i, k)$  occur. This is, in fact, the best evidence that the apparent touching of levels seen in UHF in Fig. S2(d) and S4(d) are actually avoided crossings. Had they been actual crossings,

$\bar{S}_z(i, k)$  would have changed discontinuously as functions of  $k$ .

To summarize, in UHF, levels undergo avoided crossing, and the  $\bar{S}_z(i, k)$  change smoothly as a function of  $kl$ . However, since the avoided crossings occur below  $\mu$ , the values of  $\bar{S}_z(i, k)$  at the  $\mu$ -crossing,  $\bar{S}_{z\mu}(i)$ , do change discontinuously through the transition as shown in Fig. 1(e) and Fig. 1(f) of the main text.

Finally, let us look at Fig. S3(c) and S5(c). These show the average of the electronic charge density close to the spin-mode-switching transition, but on either side of it. In Fig. S3(c), we focus on the Phase A  $\rightarrow$  Phase B transition. It is seen that the electronic charge density hardly changes across the transition. The same is true of the Phase A  $\rightarrow$  Phase C transition in Fig. S5(c). This is the basis of our conclusion in the main text that the spin-mode-switching transitions are not primarily driven by charge effects, but rather primarily by spin-exchange effects.

Fig. S6(a)-(c) show the single particle energy levels in the full range of active guiding centers ( $-20 < kl < 20$ ) in Phases A, B and C. We note that the occupations and dispersions converge to the expected values in the bulk (on the left) and in the vacuum (on the right) in all three cases shown here and for all values of  $W$  considered in this work.

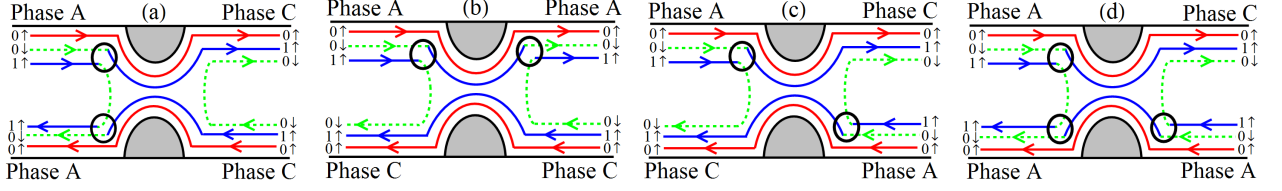


FIG. S10. (Color online) A single QPC tuned at the  $g_2 = 2$  plateau, connecting regions with different confining potentials. In this figure  $\bar{E}_c > 2.13$ , hence the smooth edges are in Phase C, and the  $\nu = 2$  QPC region is fully polarized. The two outer edge modes carry the current. If the source is at the top left (Phase A), no disorder-induced tunneling can take place between any pair of neighboring modes to the left of the QPC. If the source is at the bottom right (Phase C), the innermost mode has the opposite spin of the two outer modes, and therefore disorder-induced tunneling is ineffective. Thus, the two-terminal conductance plateau at  $g_2 = 2$  is not undermined by disorder-induced backscattering.

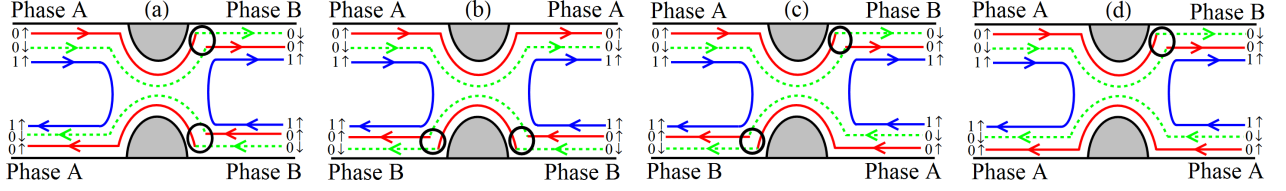


FIG. S11. (Color online) A single QPC tuned at the  $g_2 = 2$  plateau, connecting regions with different confining potentials. Here  $\bar{E}_c < 2.13$ , hence the smooth edges are in Phase B, and the  $\nu = 2$  QPC region is unpolarized. If the source is at the top left (Phase A), disorder-induced tunneling cannot degrade the current. If the source is at the bottom left, then in (a), (b), Phase B does allow disorder-induced tunneling to degrade the source current, whereas in (c), (d), Phase A does not. Thus, the setups of (a) and (b) will have a left-right asymmetry of the  $g_2 = 2$  conductance plateau, while the setups of (c), (d) will not.

### III. VARIATIONAL CALCULATION

One limitation of HF is that the ground state can only be a Slater determinant of some set of single-particle states. Thus, at  $T = 0$  the occupation of any single-particle state is either 0 or 1. To overcome this limitation,

we consider a class of variational states that allow the occupations to lie between 0 and 1 even at  $T = 0$ . These states do not conserve particle number but we choose parameters so that the average number maintains charge neutrality. To be specific, for the edge of  $\nu = 3$  we consider states of the form

$$|\psi\rangle = \prod_k (U_k + V_{0k} e^{i\theta_{0k}} c_{0k\uparrow}^\dagger + V_{1k} e^{i\theta_{1k}} c_{0k\downarrow}^\dagger c_{0k\uparrow}^\dagger + V_{2k} e^{i\theta_{2k}} c_{1k\uparrow}^\dagger c_{0k\uparrow}^\dagger + V_{3k} e^{i\theta_{3k}} c_{1k\uparrow}^\dagger c_{0k\downarrow}^\dagger c_{0k\uparrow}^\dagger) |0\rangle. \quad (\text{S15})$$

where  $U_k$ ,  $V_{ik}$  and  $\theta_{ik}$  are real numbers. Normalizing  $|\psi\rangle$  imposes the condition  $U_k^2 + \sum_i V_{ik}^2 = 1$  for each guiding center  $k$ , leaving us with 8 free parameters for each guiding center ( $V_{ik}$  and  $\theta_{ik}$ ). Note that the HF state without LL-mixing is a member of this class of states. The average occupation of each LL is,

$$\langle c_{0k\uparrow}^\dagger c_{0k\uparrow} \rangle = \sum_{i=0}^4 V_{ik}^2 \quad (\text{S16})$$

$$\langle c_{0k\downarrow}^\dagger c_{0k\downarrow} \rangle = V_{1k}^2 + V_{3k}^2 \quad (\text{S17})$$

$$\langle c_{1k\uparrow}^\dagger c_{1k\uparrow} \rangle = V_{2k}^2 + V_{3k}^2 \quad (\text{S18})$$

$$\langle c_{0k\downarrow}^\dagger c_{0k\uparrow} \rangle = 0 \quad (\text{S19})$$

$$\langle c_{1k\uparrow}^\dagger c_{0k\uparrow} \rangle = 0 \quad (\text{S20})$$

$$\langle c_{1k\uparrow}^\dagger c_{0k\downarrow} \rangle = V_{2k} V_{1k} e^{i(\theta_{1k} - \theta_{2k})} \quad (\text{S21})$$

We also note that  $|\psi\rangle$  does not allow the states of  $0\uparrow$  level to mix with those of  $0\downarrow$  or  $1\uparrow$  but allows a mixing of the latter two.

Furthermore since the particle number is not conserved we have,

$$\langle c_{0k\uparrow}^\dagger \rangle = U_k V_{0k} e^{-i\theta_{0k}} \quad (\text{S22})$$

$$\langle c_{0k\downarrow}^\dagger \rangle = V_{0k} V_{1k} e^{i(\theta_{0k} - \theta_{1k})} - V_{2k} V_{3k} e^{i(\theta_{2k} - \theta_{3k})} \quad (\text{S23})$$

$$\langle c_{1k\uparrow}^\dagger \rangle = V_{0k} V_{2k} e^{i(\theta_{0k} - \theta_{2k})} + V_{1k} V_{3k} e^{i(\theta_{1k} - \theta_{3k})} \quad (\text{S24})$$

Although  $|\psi\rangle$  is a product state and does not couple different guiding centers directly, the non-conservation of particle number produces non-zero averages for operators of the form  $O_{n_1 n_2; s_1 s_2}(k, q_x) = c_{n_1 k s_1}^\dagger c_{n_2 k + q_x s_2}$  for  $q_x \neq 0$ .

Our variational states therefore inherently violate translation invariance in the  $x$ -direction (along the edge). While one cannot avoid this, one may choose states where the *electron density* is (almost) uniform. Recalling that the electron density  $\rho_e(q_x, q_y)$  is a superposition of the operators  $O_{n_1 n_2; s s}(k, q_x)$  (see Eq. S5), we can arrange for

values of  $\theta_k$  to make  $\langle \psi | \rho_e(q_x, q_y) | \psi \rangle$  vanish. We achieve this by imposing the conditions  $\theta_{1k} + \theta_{2k} = 0 = \theta_{0k} + \theta_{3k}$  at each  $k$  and  $\theta_{0k} = k^2 / (N_p \ell^2) = \frac{1}{2} \theta_{1k}$  where  $N_p$  is a large prime number. There remain 4 variational parameters ( $V_{ik}$ ) for each guiding center. To find the ground state, we need to minimise the energy functional  $\mathcal{F}[\{V_{ik}\}]$ ,

$$\mathcal{F}[\{V_{ik}\}] = \langle \psi | H | \psi \rangle + \lambda (\langle \psi | N | \psi \rangle - N_e)^2$$

where we have added a Lagrange multiplier  $\lambda$  to fix the average particle number to be  $N_e$ .

Unfortunately, with a large number of guiding centers, this is still computationally prohibitive. To make further progress, we assume that spin is a good quantum number so that  $0\downarrow$  and  $1\uparrow$  do not mix and that the occupations in the Landau levels vary smoothly, except, possibly, for a discontinuous jump at the chemical potential. The matrix elements are assumed to have the functional form

$$\langle c_{1k\uparrow}^\dagger c_{0k\downarrow} \rangle = 0 \quad (\text{S25})$$

$$\langle c_{0k\uparrow}^\dagger c_{0k\uparrow} \rangle = \begin{cases} \frac{1}{2} [1 - \tanh(\alpha_1(k - K_1 - \beta_1))] & \text{if } k \leq K_1 \\ \frac{1}{2} [1 - \tanh(\alpha_1(k - K_1 + \beta_1))] & \text{if } k > K_1 \end{cases} \quad (\text{S26})$$

$$\langle c_{0k\downarrow}^\dagger c_{0k\downarrow} \rangle = \begin{cases} \frac{1}{2} [1 - \tanh(\alpha_2(k - K_2 - \beta_2))] & \text{if } k \leq K_2 \\ \frac{1}{2} [1 - \tanh(\alpha_2(k - K_2 + \beta_2))] & \text{if } k > K_2 \end{cases} \quad (\text{S27})$$

$$\langle c_{1k\uparrow}^\dagger c_{1k\uparrow} \rangle = \begin{cases} \frac{1}{2} [1 - \tanh(\alpha_3(k - K_3 - \beta_3))] & \text{if } k \leq K_3 \\ \frac{1}{2} [1 - \tanh(\alpha_3(k - K_3 + \beta_3))] & \text{if } k > K_3 \end{cases}, \quad (\text{S28})$$

where  $\alpha_i, \beta_i$  and  $K_i (i = 1, 2, 3)$  are 9 variational parameters. Here the bulk state is always  $|0\uparrow, 0\downarrow, 1\uparrow\rangle$  but the order of edge modes can change. The variational parameters  $K_{oi}$  denote the positions where the Landau levels cross the chemical potential, the parameters  $\beta_i$  characterize the discontinuity in the occupation of level  $i$  at  $\mu$ , while  $\alpha_i$  allow a smooth relaxation back to 0 or 1 away from the discontinuity.

To satisfy the constraint in Eq. (S25) we must have,

$$V_{2k} = 0 \text{ if } K_3 < K_2$$

$$V_{1k} = 0 \text{ if } K_3 > K_2$$

Then we can replace the remaining  $V_{ik}$  in the functional  $\mathcal{F}$  with the functional forms defined above. The new functional  $\mathcal{F}[\{\alpha, \beta, K\}]$  is then minimised using the method of steepest descent.

In the absence of exchange interaction, the energy functional is dominated by the classical Coulomb interaction between electron density and background density. Therefore, if we vary the strengths of the direct ( $E_{cd}$ ) and exchange ( $E_{cx}$ ) terms independently and set

$E_{cx} = 0$ , the occupations can be expected to change very smoothly from 1 to 0 so as to make the electron density completely cancel the background density. Indeed we find that in this regime, our variational calculation gives  $\beta_i = 0$ , implying a continuous variation of occupations, as shown in Fig. S7. As the exchange interaction is increased in strength, the smoothly varying  $n(k)$  revert back to the HF solution with  $n(k) = 0, 1$ . As explained in the main text, mode-switching is an exchange-driven effect and only occurs if the exchange interaction is larger than a certain minimum fraction of the direct interaction. We find that in the regime where HF shows spin-mode-switching, the variational calculation always gives the HF state as the ground state, whereas in the regime where the occupations vary smoothly, there is no spin-mode-switching.

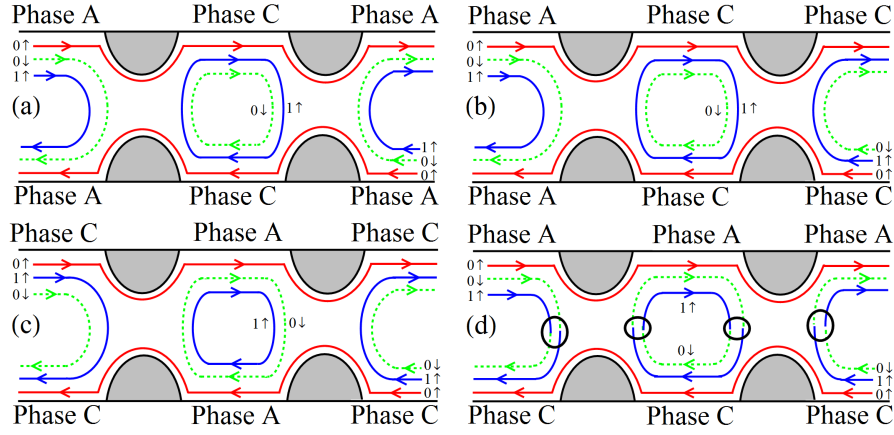


FIG. S12. (Color online) A two-QPC setup tuned at the  $g_2 = 1$  plateau connecting regions with different confining potentials. Here  $\tilde{E}_c > 2.13$ , which implies that the smooth edges are in Phase C. All 3 incoming modes on the left or right section are biased while in the middle section only the outer ( $0\uparrow$ ) mode is biased. Following the reasoning presented in the text, we see that in (a,b) disorder induced backscattering is possible, while in (c,d) edge-to-edge backscattering cannot take place.

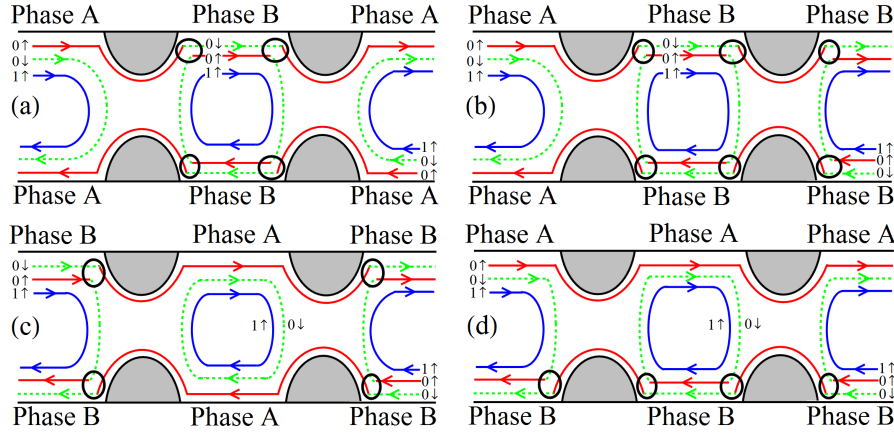


FIG. S13. (Color online) A two-QPC setup tuned at the  $g_2 = 1$  plateau connecting regions with different confining potentials. Here  $\tilde{E}_c < 2.13$ , implying that the smooth edges are in Phase B. In the middle section only the ( $0\uparrow$ ) mode is biased. (a,b) Disorder induced backscattering is possible. (c,d) Edge-to-edge backscattering cannot take place.

#### IV. EXPERIMENTAL SIGNATURES

Edge modes play a crucial role in transport in quantum Hall states. It is therefore expected that signatures of spin-mode-switching will be manifested in transport experiments. While the total Hall conductance of the  $\nu = 3$  state is fixed by the bulk topology, signatures of mode-switching can be expected to show up in constrained geometries with quantum point contacts (QPCs) when only some of the edge modes are allowed to go through. Here again there are two classes of signatures, those that require measuring the spin-polarization of the current, and those that do not.

The spin-dependent signatures have been discussed sufficiently in the main text, so we will focus here on signatures of spin-mode-switching that depend on the effects of disorder in one- and two-QPC setups. As men-

tioned in the main text, nonmagnetic disorder allows tunneling between neighboring chiral channels of the same spin. We make the simplifying assumption that if two  $\uparrow$  channels separated in space have a  $\downarrow$  chiral channel between them, no tunneling occurs between the  $\uparrow$  channels.

We will show that disorder can induce a left-right asymmetry in the plateau of the tunneling conductance in a single-QPC geometry when spin-mode-switching has occurred on (say) the right side of the QPC, but not the left. The asymmetry pertains to the current source being either in edge Phase A (not mode-switched), or in the edge spin-mode switched phase.

Consider a Hall bar with a single QPC connecting regions of the sample below (Phase A) and above (Phase B/C) the switching transition as shown in Fig. S8 - S11. When the QPC is open (no constriction), the 2-terminal conductance is  $g_2 = 3$  (in units of  $\frac{e^2}{h}$ ). Let us now pinch

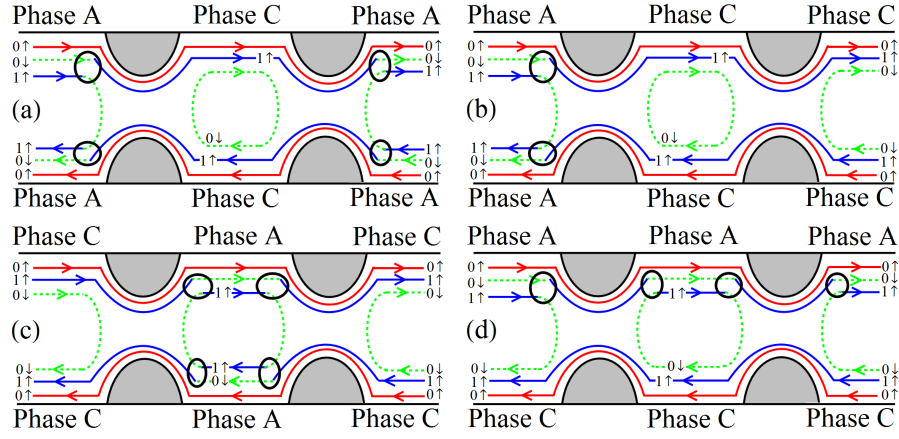


FIG. S14. (Color online) The same potential configuration as in Fig. S12(a), at the  $g_2 = 2$  plateau. Here  $\bar{E}_c > 2.13$ , implying that the smooth edges are in Phase C, and the QPC regions are fully polarized. The reasoning explained in the text indicates that disorder-induced backscattering cannot take place.

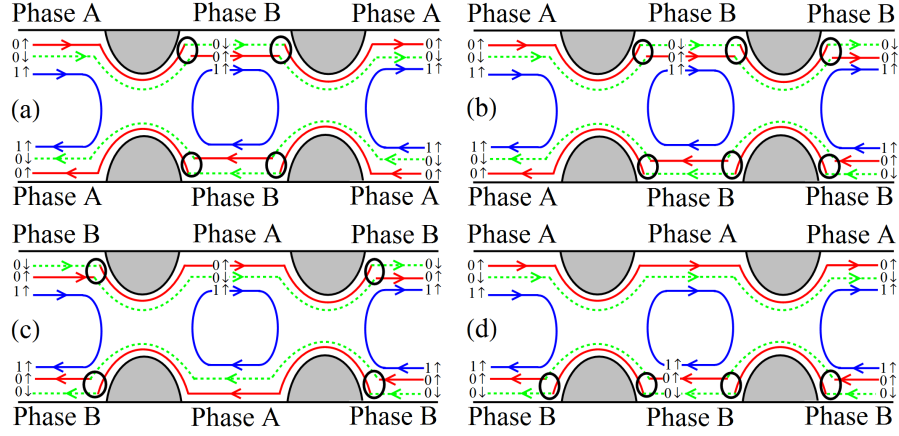


FIG. S15. (Color online) The same potential configurations as in Fig. S13, at the  $g_2 = 2$  plateau. Here  $\bar{E}_c < 2.13$ , implying that the smooth edges are in Phase B, and that the QPC regions are unpolarized. The reasoning explained in the text indicates that disorder-induced backscattering can take place in the setups shown in (a,b).

off the QPC potential, and consider first  $g_2 = 1$  configurations, shown in Fig. S8 and S9, which depict the cases  $\bar{E}_c > 2.13$  and  $\bar{E}_c < 2.13$  respectively. For some of these configurations spin hybridization at the QPC is required (it is marked by a circle): there is no spin hybridization in Fig. S8(a), a single one in Fig. S8(d), S9(d), and two in Fig. S8(b), S8(c), S9(a)-(c) each. Let us now introduce weak (non-magnetic) static disorder which allows for tunneling between neighbouring same-spin edge modes. We then voltage bias, for each configuration, the outermost incoming mode, either on the top left or on the bottom right. For the setup of Fig. S8(a), when the bias is put on the left-moving chiral ( $0\uparrow$ ) (lower right), the current can partially tunnel to the neighbouring ( $1\uparrow$ ) mode and eventually be backscattered, resulting in degradation of the quantized  $g_2 = 1$  value. This will not be the case if the bias is put on the right-moving ( $0\uparrow$ ) mode (upper left). The result is a disorder-induced breaking of

left-right symmetry of electric transport. That will apply to the setup depicted in Fig. S8(b) as well, but not Fig. S8(c) and Fig. S8(d). On the other hand, for all the setups in Fig. S9, the outermost and middle incoming modes have opposite spins. Therefore, disorder induced tunneling between like spin modes is not possible in this case and the quantized  $g_2 = 1$  value will not suffer from presence of disorder.

By somewhat opening the QPC, we may tune the system to be at the  $g_2 = 2$  plateau. First we consider the case when  $\bar{E}_c > 2.13$  (depicted in Fig. S10), which implies that the smooth edges are in Phase C, and that the QPC region is fully polarized. Such configurations require that spin hybridization takes place at two or more different points near the QPC. Following the same logic as in the previous paragraph, we see that disorder-generated tunneling between like-spin channels will not give rise to back-scattering, regardless of where the source and drain

are. This means that conductance quantization is robust and has no left-right asymmetry.

Still staying with  $g_2 = 2$ , we now consider the case when  $\tilde{E}_c < 2.13$  (depicted in Fig. S11), which implies that the smooth edges are in Phase B, and that the QPC region is unpolarized. In this case, when the source is located in the region where the edge is in Phase A, no disorder-induced backscattering takes place. However, if the source is in the region where the edge is in Phase B, disorder-induced backscattering can degrade the conductance. Thus, depending on the particular configuration of edges, there can be a left-right asymmetry in the quality of the conductance plateau.

Next, we analyze a 2-QPC setup, depicted in Fig. S12-S15. We consider the case where the QPCs are pinched so as to obtain a  $g_2 = 1$  plateau (Fig. S12 and S13). In the region between the two QPCs only the  $(0\uparrow)$  mode is biased. If the potential on both edges in the middle section is made smooth, disorder induced tunneling from

$(0\uparrow)$  to the  $(1\uparrow)$  channel on one edge, and from  $(1\uparrow)$  to the  $(0\uparrow)$  on the other edge, may take place (Fig. S12(a),(b) and S13(a),(b)). The quality of the  $g_2 = 1$  plateau is undermined due to this edge-to-edge backscattering. There is no backscattering when either of the middle section edges is sharp (Phase A) (Fig. S12(c),(d) and S13(c),(d)). For the same configurations, with the QPCs slightly more open ( $g_2 = 2$ , cf. Fig. S14, S15), we note that backscattering will only take place in the setups shown in Fig. S15(a),(b).

---

- [1] J. Dempsey, B. Y. Gelfand, and B. I. Halperin, Phys. Rev. Lett. **70**, 3639 (1993).
- [2] C. de C. Chamon and X.-G. Wen, Phys. Rev. B **49**, 8227 (1994).
- [3] T. Jungwirth and A. H. MacDonald, Phys. Rev. B **63**, 035305 (2000).
- [4] E. H. Rezayi, T. Jungwirth, A. H. MacDonald, and F. D. M. Haldane, Phys. Rev. B **67**, 201305 (2003).